MNRAS **462,** 1329–1340 (2016)
Advance Access publication 2016 July 18
doi:10.1093/mnras/stw1723

The role of gas infall in the evolution of disc galaxies

Mercedes Mollá,[1★] Ángeles I. Díaz,[2,3] Brad K. Gibson,[4★] Oscar Cavichia[5] and Ángel-R. López-Sánchez[6,7]

[1]*Departamento de Investigación Básica, CIEMAT, Avda. Complutense 40, E-28040 Madrid, Spain*
[2]*Universidad Autónoma de Madrid, E-28049 Madrid, Spain*
[3]*Astro-UAM, Unidad Asociada CSIC, Universidad Autónoma de Madrid, E-28049 Madrid, Spain*
[4]*E.A. Milne Centre for Astrophysics, University of Hull, Hull HU6 7RX, United Kingdom*
[5]*Instituto de Física e Química, Universidade Federal de Itajubá, Av. BPS, 1303, 37500-903 Itajubá-MG, Brazil*
[6]*Australian Astronomical Observatory, PO Box 915, North Ryde, NSW 1670, Australia*
[7]*Department of Physics and Astronomy, Macquarie University, NSW 2109, Australia*

Accepted 2016 July 14. Received 2016 July 13; in original form 2016 March 14

ABSTRACT

Spiral galaxies are thought to acquire their gas through a protracted infall phase resulting in the inside-out growth of their associated discs. For field spirals, this infall occurs in the lower density environments of the cosmic web. The overall infall rate, as well as the galactocentric radius at which this infall is incorporated into the star-forming disc, plays a pivotal role in shaping the characteristics observed today. Indeed, characterizing the functional form of this spatio-temporal infall *in situ* is exceedingly difficult, and one is forced to constrain these forms using the present day state of galaxies with model or simulation predictions. We present the infall rates used as input to a grid of chemical evolution models spanning the mass spectrum of discs observed today. We provide a systematic comparison with alternate analytical infall schemes in the literature, including a first comparison with cosmological simulations. Identifying the degeneracies associated with the adopted infall rate prescriptions in galaxy models is an important step in the development of a consistent picture of disc galaxy formation and evolution.

Key words: galaxies: formation – galaxies: ISM – galaxies: spiral.

1 INTRODUCTION

Numerical chemical evolution models (CEMs) are one of the most flexible (and long-standing) tools for interpreting the distribution of metals in both the gas and stellar phases of galaxies. The power of CEMs lies in the rapid and efficient coupling of star formation and feedback prescriptions, with the stellar nucleosynthesis, initial mass function formalisms, and treatments of gas infall/outflow. While lacking a self-consistent (hydro-)dynamical treatment, the ability to explore these parameter spaces on computing time-scales of minutes rather than months, ensures CEMs maintain a prominent role in astrophysics today.

The initial motivation for the development of CEMs was the identification of what is now known as the *G-dwarf problem* (van den Bergh 1962; Schmidt 1963; Lynden-Bell 1975); specifically, there is an apparent paucity of metal-poor stars in the solar neighbourhood, relative to the number predicted to exist should the region behave as a 'closed-box', i.e. one in which gas neither enters nor departs. It was recognized that a viable solution to the G-dwarf problem lay in the relaxation of this closed-box assumption, via the inclusion of a gas infall prescription (Larson 1972; Edmunds 1990). The infall of metal-poor gas can then dilute the existing elemental abundances, whilst simultaneously increasing the early star formation rate (SFR), thus producing a stellar metallicity distribution shifted to moderately higher metallicities. Moreover the star formation sustained by metal-poor gas accretion self-regulates to produce a constant gas-phase metallicity close to the stellar yield (i.e. close to the solar metallicity). The G-dwarf problem also appears in external galaxies, as M 31 (Worthey, Dorman & Jones 1996). Building on this framework, most classical models of disc formation assume a protogalaxy or dark matter halo which acts as the source of the infalling gas (Güsten & Mezger 1983; Lacey & Fall 1983, 1985; Matteucci & Francois 1989; Portinari, Chiosi & Bressan 1998) without which, in addition, radial abundance gradients are increasingly difficult to recover.[1]

★E-mail: mercedes.molla@ciemat.es (MM); Brad.Gibson@hull.ac.uk (BKG)

[1] Some more recent models include two or even three infall phases, each corresponding in turn to the formation of the halo, followed by that of the thick and thin discs (Chiappini, Matteucci & Romano 2001; Chiappini,

Extensions of this classical framework include those employing a multiphase representation for the interstellar medium (Ferrini et al. 1992, 1994; Mollá, Ferrini & Díaz 1996). In Mollá & Díaz (2005), we calculated a generic grid of theoretical CEMs, defined in terms of their rotation velocity using the universal rotation curve (URC) of Persic, Salucci & Stel (1996). In that work we assumed that the infall rate, or its inverse, the collapse time-scale, τ_c, for each galaxy, depends on the total mass of each theoretical galaxy, with the low mass galaxies forming on a longer time-scale than the massive ones, according to the expression $\tau_c \propto M^{-1/9}$ (Gallagher, Hunter & Tutukov 1984). Such a mass-dependence mimics the downsizing phenomenon now associated with galaxy formation (Heavens et al. 2004; Pérez-González et al. 2008).

These sorts of adopted time-scale relationships are, however, weakly constrained in the sense that they were only implemented to ensure present-day abundance patterns and gas fractions were recovered. We now possess much more information pertaining to the manner by which gas moves from the cosmic web, through haloes, and on to discs, and so more realistic prescriptions should be pursued.

From the observational point of view, the observations of the atomic hydrogen line H I at 21 cm in nearby galaxies revealed the existence of extensive haloes containing gas up to 15 kpc above the plane of the discs (e.g. Fraternali et al. 2002; Barbieri et al. 2005; Boomsma et al. 2008; Heald et al. 2011; Gentile et al. 2013). This gas could be deposited on the discs, forming at present the reservoirs from which stars form in the outer parts of galaxies. In fact, it seems to be rotating slower than in discs and moving slowly towards inwards (Oosterloo 2004). However, most of observational evidences of gas accretion are indirect, since this gas is tenuous. Only the high velocity clouds (HVCs) are well studied (e.g. Wakker, van Woerden & Gibson 1999), their existence being in agreement with theoretical expectations. Richter (2006) analysed the HVCs in the local intergalactic medium suggesting, in agreement with previous findings from Blitz et al. (1999), that these HVC's are the building blocks of galaxies, and situated within the halo at galactocentric distances less than ∼40 kpc, consistent with the predictions of cosmological hydrodynamical simulations (Connors et al. 2006). These clouds are comprised of low-metallicity gas (e.g. Gibson et al. 2001), consistent with the material being the fuel out of which the disc forms. It should also be noted that there now exists recent observations which suggest the infall of low-metallicity H I gas in dwarf galaxies triggering star formation therein. The most prominent example is NGC 5253, but additional examples are described by López-Sánchez (2010); López-Sánchez et al. (2012, and references therein).[2]

Oosterloo (2004) estimated that, if bumps of H I gas have a total mass of order 10^{8-9} $M_\odot$ and are accreted in 10^{8-9} yr, the typical accretion rate would be ∼1 $M_\odot$ yr^{-1}. On the other hand, Sancisi et al. (2008), reviewing all data referring this subject of gas around galaxies and its possible movement towards them, infer a mean visible accretion rate of cold gas of at least 0.2 $M_\odot$ yr^{-1}, which should be considered a lower limit of the infall rate; such a value poses a problem when it compared with the SFR, since it is roughly one order of magnitude smaller than necessary to sustain the observed SFR (see Sánchez Almeida et al. 2014a, and references therein). The Sancisi et al. (2008) value is, however, calculated using only the cold gas, neglecting the likely more dominant background reservoir of ionized gas. Lehner & Howk (2011) measuring the mass of this phase, estimating the infall rate increases to ∼0.8 $M_\odot$ yr^{-1}. Later, Richter (2012) gives an infall rate of 0.5–0.7 $M_\odot$ yr^{-1} as an estimate for the Milky Way Galaxy (MWG) and the Andromeda galaxy (M 31) within a radius of 50 kpc, claiming that 'in MWG and other nearby galaxies the infall of neutral gas may be observed directly by H I 21 cm observations of extra-planar gas clouds that move through the haloes'. Very recently, Fernández et al. (2016) report the H I 21 cm detection in emission at a redshift $z = 0.375$ with the COSMOS H I Large Extragalactic Survey. Following these data, the diffuse gas is M(H I) = 2×10^{10} $M_\odot$, the molecular one is M(H_2) = 1.8–9.9 × 10^{10} $M_\odot$, and the stellar mass $M_* = 8.7 \times 10^{10}$ $M_\odot$. This implies that the disc of this galaxy accreted [13–22] × 10^{10} $M_\odot$ in ∼8 Gyr, which will produce an averaged value for the infall rate of 17–27 $M_\odot$ yr^{-1}. Although these numbers are highly speculative, given the lack of any more firm estimates, we will employ them in this work.

Additional guidance regarding infall rates can be provided by tracing the spatial and temporal infall of gas on to discs, via the use of cosmological simulations. This cosmological gas supply has a strong dependence on redshift and halo mass. However, the interplay between the circumgalactic gas components is not well known and the gas physics in a turbulent multiphase medium is non-trivial to capture in (relatively) low-resolution hydrodynamical simulations. The consequence is that there remain only select examples in the literature which reproduce successfully and simultaneously (both in terms of size and relative proportions) the characteristics of late-type discs and their spheroids (e.g. Brook et al. 2012b; Vogelsberger et al. 2013; Schaye et al. 2015). Bearing in mind this cautionary statement, it is interesting to note that these simulations suggest that most of the baryons in galaxies are accreted diffusely, with roughly 3/4 due to smooth accretion, and 1/4 from mergers.

Recently, Brook et al. (2014) have generated a suite of cosmological simulations which reproduce the gross characteristics of the Local Group. Analysing these simulations, they find the relationship between the stellar mass and the halo mass (their fig. 2 and equation 2), valid for a stellar mass range [10^7–10^8] $M_\odot$. In the last decade, several techniques have been developed to obtain such a relation between the dynamical mass in the proto-haloes and the baryonic mass in the discs, although usually this last one is associated with the stellar mass. One of these statistical approaches connecting the cold dark matter (CDM) haloes with their galaxies is the sub-halo abundance matching technique. With that, the total stellar-to-halo mass relation (SHMR) is obtained (Shankar et al. 2006; Behroozi, Conroy & Wechsler 2010; Guo et al. 2010; Rodríguez-Puebla, Drory & Avila-Reese 2012; Behroozi, Wechsler & Conroy 2013; Rodríguez-Puebla et al. 2015). Other formalisms use the halo occupation distribution, which specifies the probability that a halo of mass M has a given number of galaxies with a certain mass M_* (or luminosity, colour or type). As a result, the SHMR is also estimated (Leauthaud et al. 2010; Moster et al. 2010; Yang et al. 2012). A summary of these results can be found in fig. 5 of Behroozi et al. (2013). This relation constrains the possible accretion of gas from the halo to the discs.

One of the questions that arises when cosmological simulations and data are compared is, such as Kormendy & Freeman (2016) states, that there is a collision between the cuspy central density seen in cosmological simulations and the observational evidence that galaxies have flat cores. This tension there exists from some

Matteucci & Meynet 2003; Fenner & Gibson 2006; Micali, Matteucci & Romano 2013).

[2] Similarly, it has been suggested that the high N/O ratio found in some of these galaxies might be also related to infall of metal-poor gas. See the excellent review by Sánchez Almeida et al. (2014a) for details.

years ago and it is still present. The use of a Navarro, Frank and White (1996) (NFW) profile, with its $\rho \propto r^{-1}$ producing cusps at small radii, comes from the era in which cosmological simulations were undertaken primarily only with dark matter, but it continues be widely used. Over the past years the data for rotation curves (RCs) have improved immensely, as well as the mass modelling, showing that most of dwarf disc galaxies have cored haloes. Although it seemed less clear for giant spirals, Donato et al. (2009) analysed RCs for a sample of 1000 galaxies finding a good fit of a core-halo profile to the data, better than the one for the NFW. More recently, Nesti & Salucci (2013) have carefully analysed the available data for the MWG, fitting both dark matter Burkert and NFW profiles. They find that the cored profile produces the best result, and is therefore the preferred one, claiming that this is in agreement with similar fits obtained for other external disc galaxies and in agreement with the mass model underlying the URC. Ogiya et al. (2014) and Ogiya & Mori (2014) say that this discrepancy between observations and simulations may be due to dynamical processes that transform a cuspy into a cored model, probably by the effect of the feedback that modifies the star formation process at small scale. In fact, most recent cosmological simulations (see Brook et al. 2012b) which include this feedback in the star formation prescriptions, find that this transformation occurs when there is violent feedback from rapid star formation in the inner regions of disc galaxies. In this work we use the Salucci et al. (2007, hereinafter SAL07) expressions, who use the URC formalism assuming that halo distributions follow a Burkert core isothermal profile.

In this work, we compute the infall rate for a set of theoretical galaxies with total dynamical masses in the range $M_{\rm vir} \sim [5 \times 10^{10}$–$10^{13}]$ $M_\odot$. Following the prescriptions of SAL07, we derive the RCs for each halo and disc, and their corresponding radial mass distributions. By imposing that gas from the halo falls on to the discs at a rate such that after a Hubble time the systems end with masses as observed in nature, we obtain the infall rate for each galaxy and for each radial region therein. We analyse the infall rate resulting from these prescriptions, comparing with the results from assumptions of previous CEMs, those inferred from cosmological simulations, and those from extant empirical data concerning mass accretion. We pay special attention to the redshift evolution of this infall in galaxies of different dynamical masses, and analyse its radial dependency within individual galaxies. We verify that the final halo–disc mass relation follows the prescriptions given by the authors cited above. The chemical evolution is beyond the scope of this work; here, we focus specifically on the manner by which gas reaches the disc. The impact on star formation and metal enrichment is the focus of the next phase of our collaboration (Mollá et al., in preparation).

We describe the framework of our models in Section 2. The results are outlined in Section 3, sub-dividing the study of the dependence of the infall rate on the galactocentric radius in Sub-section 3.1, the dependence on mass of the whole galaxies in Sub-section 3.2, and the resulting growth of the spiral discs in Sub-section 3.3. These results and their implications are discussed in Section 4. Our conclusions are summarized in Section 5.

2 MODEL FRAMEWORK

For our calculations we use the SAL07 equations, the details for which are outlined in that work. These authors combine kinematic data of the inner regions of galaxies with global observational properties to obtain the URC of disc galaxies and the corresponding mass distributions. For that they use a universal halo density profile following Burkert (1995), while the disc is described by the classical Freeman (1970) surface density law. With both components, they compute the two RCs that contribute to the total. Using data from RCs for around 1000 disc galaxies, and fitting them to the above described theoretical RC, they estimated the URC and correlations between the observational properties and the parameters defining those RCs. These are the expressions given and used here. The SAL07 work is the continuation of that of Persic et al. (1996), with the difference being that now the results are given directly as functions of $M_{\rm vir}$, instead of any other observational quantity.

We start by assuming an initial mass of gas in a spherical region or protogalaxy. The total dynamical masses for our theoretical galaxies are taken in the range $M_{\rm vir} = [5 \times 10^{10} - 10^{13}]$ $M_\odot$, with values starting at $\log M_{\rm vir} = 10.75$, increasing in mass in steps of $\Delta \log M_{\rm vir} = 0.15$, resulting in a total set of 16 models.

For each $M_{\rm vir}$, the virial radius, $R_{\rm vir}$, is computed. The latter is defined as being the radius corresponding to the transition between the virialized matter of a given halo and that of the infalling material; formally, this corresponds to: $R_{\rm vir} = 259\,(M_{\rm vir}/10^{12}\,{\rm M}_\odot)^{1/3}$ kpc.

To link the virial mass with the baryonic mass in the disc, $M_{\rm D}$, the relationship from Shankar et al. (2006, hereinafter SHAN06) is used:

$$M_{\rm star}\,[{\rm M}_\odot] = 2.3 \times 10^{10} \frac{\left(M_{\rm vir}/3.10^{11}\,{\rm M}_\odot\right)^{3.1}}{1 + \left(M_{\rm vir}/3.10^{11}\,{\rm M}_\odot\right)^{2.2}}. \quad (1)$$

In order to obtain the final baryonic disc mass, $M_{\rm D}$, it is necessary to include the mass tied up in the gas phase. From SHAN06, the atomic gas mass is related with the B-band luminosity,[3] and therefore with the stellar mass, as: $\log M_{\rm H\,I} = 2.42 + 0.675\ \log M_{\rm star}$; through these relationships, we compute $M_{\rm D} = M_{\rm star} + 1.34 \times M_{\rm H\,I}$.[4]

Both the virial and disc masses possess an intrinsic radial distribution, and therefore, following again SAL07, we use the RCs to compute their respective radial dependencies, as:

$$V^2(R) = V_{\rm H}^2(R) + V_{\rm D}^2(R) \quad (2)$$

$$V_{\rm H}^2(R)\,({\rm km\,s^{-1}}) = 6.4G\frac{\rho_0 R_0^3}{R}\left\{\ln\left(1+\frac{R}{R_0}\right) - \arctan\frac{R}{R_0} + \frac{1}{2}\ln\left(1+\frac{R^2}{R_0^2}\right)\right\}, \quad (3)$$

where ρ_0 is the central density of the halo:

$$\log \rho_0\,({\rm g\,cm^{-3}}) = -23.773 - 0.547 \log \frac{M_{\rm vir}}{10^{11}\,{\rm M}_\odot}, \quad (4)$$

and R_0 is the core radius for the Burkert profile, taken from Yegorova et al. (2012) (where equation 10 from SAL07 was updated), and given by:

$$\log R_0\,({\rm kpc}) = 0.71 + 0.547 \log \frac{M_{\rm vir}}{10^{11}\,{\rm M}_\odot} \quad (5)$$

and

$$V_{\rm D}^2(R)\,({\rm km\,s^{-1}}) = \frac{1}{2}\frac{GM_{\rm D}}{R_{\rm D}}(3.2x)^2(I_0K_0 - I_1K_1), \quad (6)$$

where $x = R/R_{\rm opt}$, the optical radius is defined as: $R_{\rm opt} = 3.2R_{\rm D}$; and I_n and K_n are the modified Bessel functions computed at $1.6x$.

[3] Similar relationships can be seen between the atomic gas mass and the R-band luminosity – e.g. fig. 8(c) of Brook et al. (2012a).

[4] In what follows, we ignore the contribution of the molecular gas component to $M_{\rm D}$.

The scalelength of the disc, R_D, is given by the expression:

$$\log R_D\,(\mathrm{kpc}) = 0.633 + 0.379 \log \frac{M_D}{10^{11}\,\mathrm{M}_\odot} + 0.069 \left(\log \frac{M_D}{10^{11}\,\mathrm{M}_\odot} \right)^2. \quad (7)$$

We define a characteristic radius for each model as $R_c = R_{opt}/2$. This radius, as R_{opt} and R_D, are, however, used only for normalization purposes, and for this work are not related to the surface brightness profile.

Having computed the components of rotation velocity, the radial mass distributions within the halo and disc components, for each value of M_{vir}, are given by:

$$M_H(< R) = 2.32\,10^5\,R\,V_H(R)^2 \quad (8)$$

$$M_D(< R) = 2.32\,10^5\,R\,V_D(R)^2. \quad (9)$$

To these two components we add a bulge component. To compute this term, we use the fact that correlations between disc and bulge structural parameters exist (Balcells, Graham & Peletier 2007; Ganda et al. 2009). From these correlations, we obtain the following expressions for the central velocity dispersion, σ_0, and the effective radius of the bulge, R_e:

$$\sigma_0\,(\mathrm{km\,s^{-1}}) = 105\,R_D^{0.54}, \quad (10)$$

$$R_e\,[\mathrm{kpc}] = 0.32\,R_D - 0.045. \quad (11)$$

Then:

$$M_{bulge}(\mathrm{M}_\odot) = 2.32\,10^5 \sigma_0^2\,R_e, \quad (12)$$

and

$$M_{bul}(R)(\mathrm{M}_\odot) = 2.32\,10^5 [\sigma_0\,e^{-R/R_e}]^2\,R. \quad (13)$$

In the central region ($R = 0$), we have also added the mass corresponding to the supermassive black hole, M_{BH}, following the classical expression: $\log M_{BH} = \beta \log(\sigma/220) + \alpha$, with $\alpha = 8$ and $\beta = 4$ (Chan 2013).

Finally, we then have:

$$M_{tot}(R) = M_D(R) + M_H(R) + M_{bul}(R). \quad (14)$$

The 16 calculated models would produce discs with baryonic masses M_D in the range $\sim[2.3 \times 10^8 - 5.5 \times 10^{11}]$ $\mathrm{M}_\odot$. The observed galactic masses for which SAL07 estimated the relations used here, lie between 10^9 and 2×10^{11} $\mathrm{M}_\odot$. Therefore, the first two models have lower masses (2.3 and 5.6×10^8 $\mathrm{M}_\odot$, respectively) outside this range. On the massive end of the spectrum, we have $\sim$3 models with masses above this limit, which could therefore be considered more appropriately as spheroids or lenticulars. As such, some caution should be applied when considering the mass extrema of our models.

Table 1 summarizes the characteristics of the radial mass distributions, obtained from the above expressions, that define our theoretical protogalaxies. For each model with number N (column 1), we give the logarithm of the virial mass, which is used to name each model, and the value of this mass, M_{vir} in columns 2 and 3; the mass the disc would have at the end of the evolution, M_D, is listed in in column 4; the mass of the bulge, M_{bul}, in column 5; the virial radius, R_{vir}, in column 6; the disc scalelength, R_D, the optical radius, R_{opt}, and the characteristic radius, R_c, are in columns 7–9. The value of the collapse time-scale at the characteristic radius, τ_c, (see next subsection) is in column 10; the maximum rotation velocity of the disc for each model, V_{rot}, in column 11; the velocity dispersion, σ_0, at the centre of the bulge in column 12; and the effective radius of the bulge, R_e, in column 13.

The total mass radial distributions $M(R)$ are represented in Fig. 1 for selected values of M_{vir} labelled with their logarithm values in panel (a). In panel (b) we show the mass included in each radial region, which would be a cylindrical region above and below the corresponding annulus in the disc or equatorial plane in which the gas will fall; that is, $\Delta M_{tot}(R) = M_{tot}(<R) - M_{tot}(<R-1)$.

3 INFALL RATES

3.1 The infall rate radial distributions: prescriptions for the collapse time-scale

We assume that the total mass is initially in a spherical region in the gas phase, from which it 'falls' from the halo on to the equatorial plane. As a consequence of this infall, the disc is formed at a characteristic time-scale called the 'collapse time-scale', $\tau_{coll}(R)$, defined as the time necessary for the disc mass $M_D(R)$ to reach

Table 1. Characteristics of the theoretical galaxies modelled in this work.

N	Name	M_{vir} (10^{10} $\mathrm{M}_\odot$)	M_D (10^{10} $\mathrm{M}_\odot$)	M_{bulge} (10^{10} $\mathrm{M}_\odot$)	R_{vir} (kpc)	R_D (kpc)	R_{opt} (kpc)	R_c (kpc)	τ_c (Gyr)	V_{rot} (km s^{-1})	σ_0 (km s^{-1})	R_e (kpc)
1	10.75	5.62	0.023	0.064	99.228	1.298	4.154	2.077	106.769	43.667	122.046	0.382
2	10.90	7.94	0.056	0.070	111.335	1.347	4.312	2.156	48.801	47.231	124.703	0.398
3	11.05	11.22	0.14	0.087	124.920	1.469	4.701	2.351	25.758	55.764	131.078	0.438
4	11.20	15.85	0.33	0.122	140.163	1.674	5.357	2.679	16.057	70.210	141.338	0.506
5	11.35	22.39	0.75	0.184	157.265	1.967	6.295	3.148	11.982	89.870	155.119	0.602
6	11.50	31.62	1.51	0.288	176.455	2.334	7.470	3.735	9.901	112.342	171.199	0.723
7	11.65	44.67	2.67	0.454	197.985	2.744	8.781	4.390	8.773	134.799	187.931	0.858
8	11.80	63.10	4.24	0.680	222.143	3.172	10.150	5.075	8.054	155.754	204.317	0.999
9	11.95	89.13	6.25	1.014	249.249	3.618	11.577	5.788	7.549	175.306	220.413	1.145
10	12.10	125.9	8.82	1.495	279.662	4.098	13.114	6.557	7.158	194.300	236.844	1.303
11	12.25	177.8	12.19	2.192	313.786	4.636	14.835	7.417	6.843	213.516	254.300	1.480
12	12.40	251.2	16.67	3.340	352.073	5.255	16.815	8.408	6.586	233.462	273.360	1.684
13	12.55	354.8	22.70	5.250	395.033	5.980	19.135	9.567	6.378	254.425	294.508	1.922
14	12.70	501.2	30.84	8.579	443.234	6.837	21.880	10.940	6.213	276.557	318.181	2.205
15	12.85	660.7	39.40	13.18	485.996	7.641	24.451	12.225	6.110	295.146	339.232	2.469
16	13.00	1000	56.87	27.08	557.999	9.087	29.079	14.539	5.999	324.533	374.896	2.945

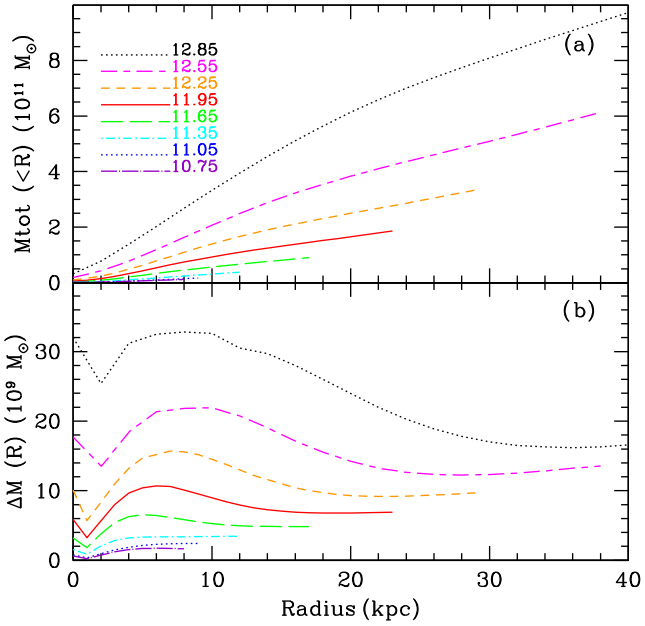

Figure 1. (a) Radial distributions of total mass $M_{\rm tot}(<R)$ for different values of virial mass $M_{\rm vir}$, given by their logarithm as labelled. (b) Radial distribution of the mass $\Delta M_{\rm tot}(R)$ within each radial region of modelled galaxies.

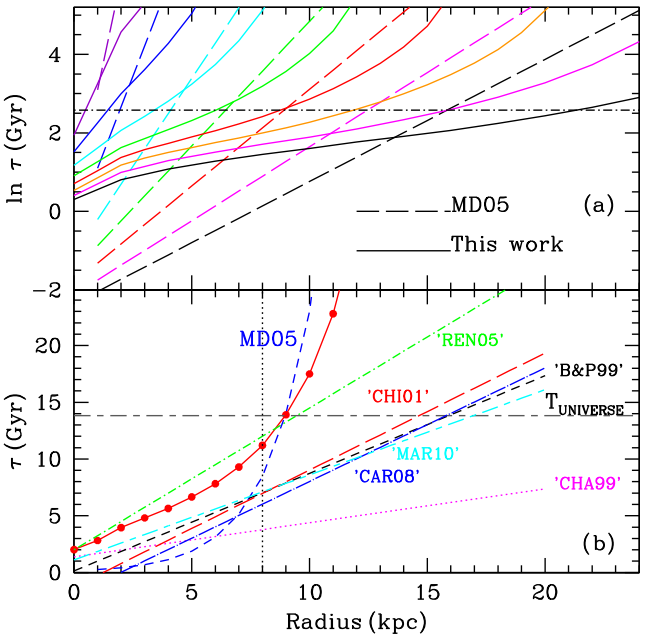

Figure 2. (a) Dependence of the collapse time-scale τ with galactocentric radius R. Each solid line represents a given radial mass distribution for a given $M_{\rm vir}$, represented with the same colours as in Fig. 1. The long dashed lines represent the radial distributions of the collapse time-scales for similar models from the MD05 grid. (b) Comparison of the radial dependence of the collapse time-scale of the most similar to MWG model, corresponding to $N = 9$, shown by the solid red line and dots for this work, compared with the old models shown by the short-dashed blue line, labelled as MD05, and with other radial functions from other authors, Chang et al. (1999), Boissier & Prantzos (1999), Chiappini et al. (2001), Renda et al. (2005), Carigi & Peimbert (2008), and Marcon-Uchida, Matteucci & Costa (2010), labelled as CHA99, B&P99, CHIA01, REN05, CAR08, and MAR10, respectively.

the actual value at the present time through the prescribed infall formalism. In other words, the halo mass decreases in a Hubble time by the exact quantity that goes into the disc via infall, integrated over each radial bin. We have already calculated the initial or total mass in the halo, $\Delta M(R)$, (see Fig. 1), in each radial region, and we also know what the corresponding $\Delta M_{\rm D}(R)$ must be. We may, therefore, calculate the collapse time for each radial region as:

$$\tau(R) = -\frac{13.2}{\ln\left(1 - \frac{\Delta M_{\rm D}(R)}{\Delta M_{\rm tot}(R)}\right)}\ ({\rm Gyr}). \qquad (15)$$

With the knowledge that the collapse time-scale depends on the dynamics of the gas, and that spiral discs possess clear radial density profiles, it should not be surprising to realize that τ will have a radial dependence. Some others have already included this radial dependence for the infall rate in their models (Lacey & Fall 1985; Matteucci & Francois 1989; Portinari et al. 1998; Boissier & Prantzos 2000; Renda et al. 2005; Fenner & Gibson 2006), by assuming different expressions. In fact, such a radial dependence is inherent to classical 'inside-out' disc formation scenarios, and is essential for obtaining the observed density profiles and radial abundance gradients. Since the mass density seems to be an exponential, we had also assumed an exponential expression for the collapse time-scale in MD05, with a steep dependence with galactocentric radius; conversely, other CEMs employed more conservative linear dependencies on galaxy radius.

The resulting radial distribution of $\tau(R)$ for this new grid is shown in Fig. 2. In panel (a), these values are shown, in logarithmic scale, for the same models as in Fig. 1, represented with the same colours and line coding. Solid lines are the results of this work, while long-dashed lines are the collapse time-scale used in MD05, for the closest model in rotation velocity. Functionally, the new (nonlinear) collapse time-scales are very different from the older ones (upper panel). The most central regions (<2 kpc) show a linear behaviour, linking the bulge with the more 'curved' expression corresponding to the disc. One can see that the inner regions have now longer time-scales compared with the MD05 prescriptions, while in the outer discs, the values are more comparable (although typically slightly shorter when compared with the older models).

In the panel (b) we show the curve corresponding to the MWG-like model, ($N = 9$) for this work, compared with our previous MD05 model for the MWG (model NDIS = 28) and other (all linear) forms drawn from the literature (and labelled accordingly). One can see that the red line (our model, here) shows longer collapse time-scales at a given radius than the other models, except for the inner disc of the Renda et al. (2005) model (although the difference between these two is minimal at these galactocentric radii).

As a consequence of this varying collapse time-scale with radius, a different infall rate is produced in each radial region, building the disc in an inside-out fashion over a Hubble time. In Fig. 3, we show the evolution with redshift (computed by following MacDonald 2006 prescriptions, as explained in Mollá et al. 2015) of the predicted infall rate, $dM_{\rm D}/dt$, for regions located at different galactocentric radii in: (a) a low mass galaxy, (b) a galaxy representing the MWG, and (c) a massive galaxy. We see that the very central regions – purple in (a) or purple and blue lines in (b) and (c) – where the bulge is located, show a strongly variable infall rate compared with the disc regions, where the curves are essentially flat until $z = 2$, and then slightly decreasing to $z = 0$. The black lines for $R = 7$, 16, and 28 kpc, in each panel (a), (b) and (d), respectively, are below the observational data. This is interesting, mainly if we take into account that the optical radius in MWG is $\sim$13 − 14 kpc; that is, the infall rate seems to define well the size of the disc. An

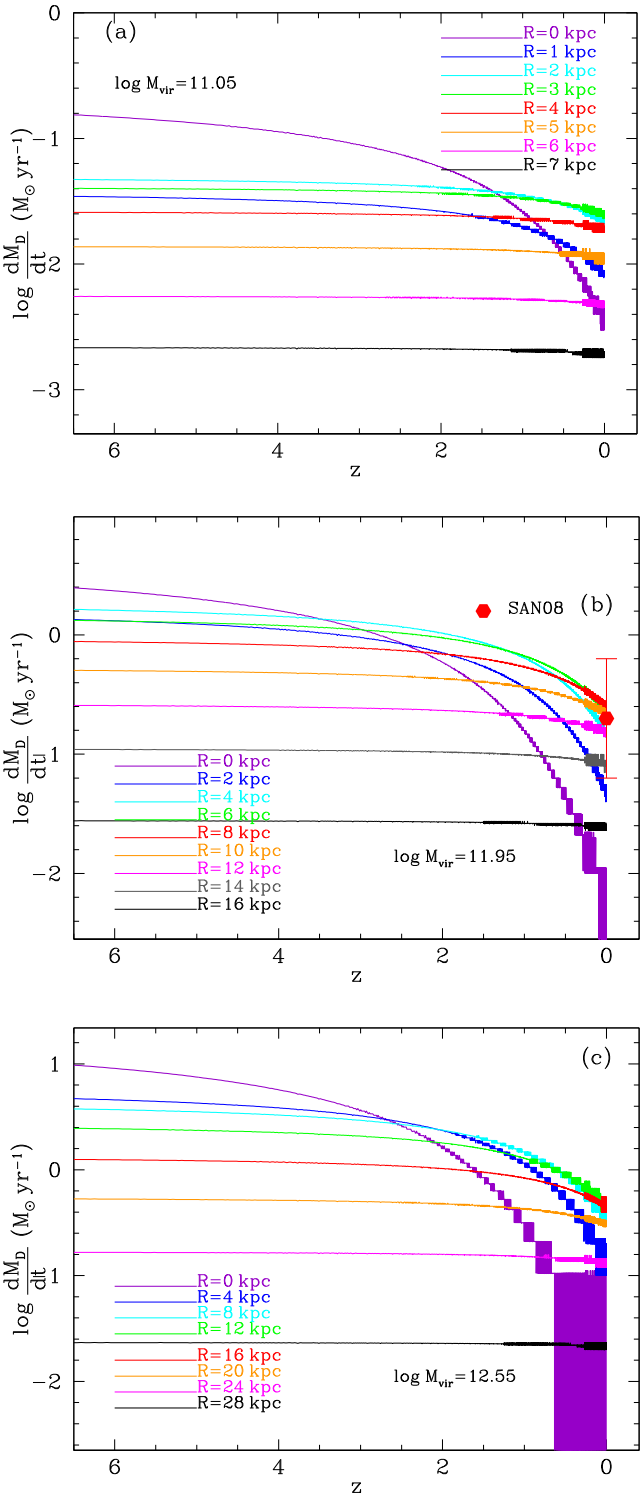

Figure 3. The infall rate in logarithmic scale as a function of the redshift z for several radial regions from the centre at the top, until the outer regions at the bottom of each panel, as labelled, in: (a) a low-mass galaxy ($\log M_{\rm vir}$ = 11.05); (b) a MWG-type galaxy ($\log M_{\rm vir}$ = 11.95); and (c) a massive galaxy ($\log M_{\rm vir}$ = 12.55). The red point with error bars is the observational estimate for the MWG (Sancisi et al. 2008).

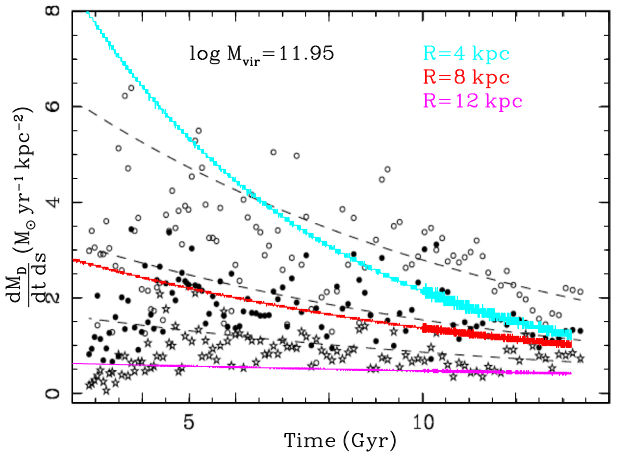

Figure 4. The time evolution of the infall rate density as (dM/dt dS) in $M_\odot$ yr^{-1} kpc^{-2} units, for three different radial regions, as labelled, compared with results from Courty et al. (2010) for galactocentric radii 4.5, 8.5, and 12.5 kpc, as open dots, filled dots, and stars, respectively. The dashed line are similar radial region results drawn from the chemical evolution model of Chiappini et al. (1997).

additional characteristic highlighted by this figure is that even with different absolute values, the infall rate behaviour is very similar in all radial regions of all discs, and clearly different to that of the bulge regions.

The comparison of the detailed infall rates from our models with cosmological simulations is not straightforward; the public availability of simulation suites such as Illustris (Nelson et al. 2015a) will aid in the future, but even that amazing data set has spatial resolution limitations which makes tracing sub-100pc disc 'impact' positions for infalling gas very difficult. And being a moving mesh, rather than particle-based, tracing the temporal history of said infalling gas is non-trivial Nelson et al. (2016). We have undertaken a cursory initial comparison though with the cosmological mesh simulation of Courty, Gibson & Teyssier (2010), as a demonstrator for what will be a more ambitious comparison in the future. For this particular simulation, the authors use multiresolved, large-scale structure, *N*-body/hydrodynamical simulations, whose initial conditions are re-centred on a Milky Way sized halo with $M_{\rm dyn} = 7.2 \times 10^{11}$ $M_\odot$. The simulations include, in addition to gravitation and gas dynamics, star formation and its associated thermal and kinetic feedback from supernovae. They identified a large reservoir of gas in the halo fuelling the disc within the virial radius, and quantified the gas accretion rate by computing the gas flowing through spherical surfaces or slabs located at different galactocentric distances (or distances above the mid-plane, in the case of slabs). In Fig. 4 we have represented our infall rates fluxes (that is, as infall rate surface densities), corresponding to $\log M_{\rm vir} = 11.95$ ($M_{\rm vir} = 8 \times 10^{11}$ $M_\odot$), as a function of time, for three radial regions located at inner, ∼solar, and outer regions, plotted with different colours, as labelled. We have included here the results from Courty et al. (2010), (their fig. 3, right-hand panel), estimated (only account for the hot gas) for three galactocentric radii of 4.5, 8.5, and 12.5 kpc, shown by open dots, filled dots, and stars, respectively, and also the results for Chiappini, Matteucci & Gratton (1997), drawn as dashed lines for similar radial regions. We see that our results reproduce the same behaviour found by cosmological simulations: a clear evolution of the infall rates decreasing with time, and also with radius at a given time. This is expected for an inside-out formation process for the galactic disc.

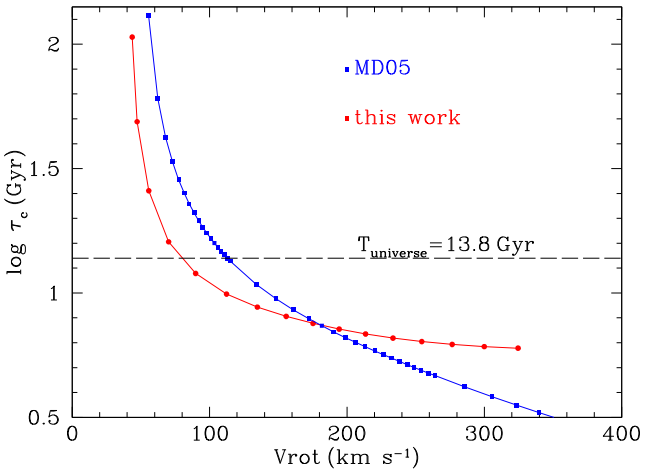

Figure 5. Relation of the characteristic collapse time-scale τ_c with the maximum rotation velocity of galaxies. The dashed (grey) line shows the time corresponding to the age of the Universe.

3.2 The dependence on the dynamical mass: the halo–disc ratio

We defined in Section 2, a characteristic radius, R_c, that we use in comparing radial mass distributions of different sizes. We have calculated the collapse time-scale for this particular radius, interpolating in the radial distributions of $\tau(R)$, thus finding the characteristic collapse time-scale, τ_c, which is in column 10 of Table 1, for each galaxy.

We plot in Fig. 5 this τ_c as a function of the maximum rotation velocity of the disc. The results of our work here (red) are compared with those employed in MD05 (blue), computed, as said, by the expression from Gallagher et al. (1984). Although a similar dependence on the total mass still appears, with shorter τ_c for massive galaxies and longer times for the low-mass galaxies, differences among both grids appear in both ends of the maximum rotation velocity range. For massive galaxies (essentially more massive than MWG), τ_c is now longer than in the older MD05 models, while it is shorter for the lower-mass galaxies.

We now integrate the infall across all radial zones to derive the infall rate for the whole disc for each galaxy. This way we may compare the total infall rate for different virial mass galaxies. Such as we see in Fig. 6, where this total infall rate for the same examples of Fig. 1 are represented as solid lines, the gas falls from the halo to the disc with a different rate depending on the total mass, as expected from Fig. 5. In panel (a) we compare these with the models from MD05 (short-dashed lines), where it is clear that the infall rate now is more constant in time and, therefore, maintains higher values (than previously) for the more massive galaxies, at the present time.

Panel (b) of Fig. 6 compares our results with the cosmological simulations presented by Dekel, Sari & Ceverino (2009) and Faucher-Giguère, Kereš & Ma (2011). Both sets of simulations are clearly more variable in time, in better agreement with our old models, but with higher absolute values. It is necessary though to note that these particular simulations lead to primarily massive spheroidal systems (rather than late-type discs). The cosmological simulations from Illustris (Nelson et al. 2015a) produce discs more similar to those observed in nature. In Nelson et al. (2015b), the team analyse how galaxies acquire their gas in simulations, with and without feedback. They found that the time taken for the gas to cross the virial radius increases by a factor of ∼2 to 3 in the presence of feedback, but is independent of the halo mass (being in the range

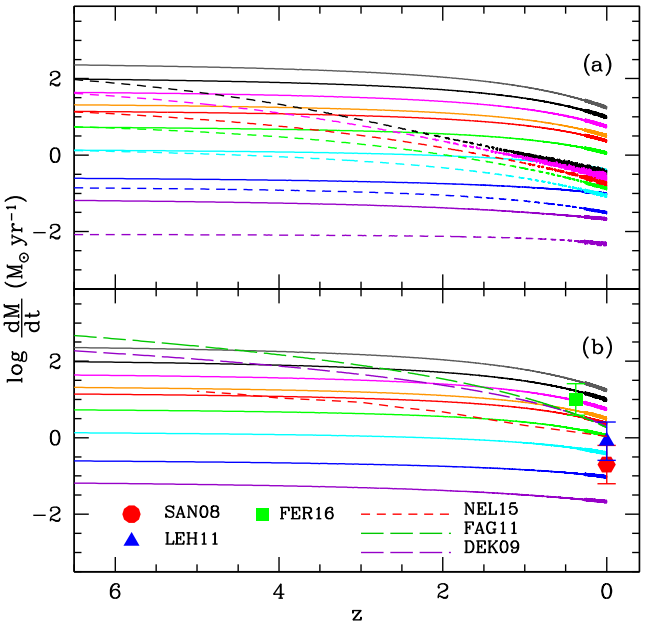

Figure 6. The infall rate as a function of the redshift z for galaxies of several virial mass, with the same coding as Fig. 1. (a) comparison with MD05 infall rates shown by short-dashed lines. (b) comparison with cosmological simulations, as long-dashed lines, from Dekel et al. (2009, DEK09) and Faucher-Giguère et al. (2011, FG11), and as short-dashed line from Nelson et al. (2015b, NEL15), as labelled. The solid red pentagon is the estimated value from Sancisi et al. (2008) while the blue triangle is given by Lehner & Howk (2011). The green square is obtained from Fernández et al. (2016) for the highest redshift galaxy observed in H I.

10^{10}–10^{12} $M_\odot$), as we also found. Using their fig. 8, we plot in Fig. 6 the redshift evolution of the non-feedback simulation. We see that these results show a much lower infall rate than the old spherical galaxy simulations, and more in agreement with our (slightly) flatter models. It is necessary to be clear, however, that this line corresponds to the accretion corresponding to a virial mass $\log M_{\rm vir} = 11.30$; that is, it may be compared with our cyan line, which lies below. It implies that this model will create a more massive disc than ours' for the same virial mass. We have also shown the standard value of the infall rate obtained for the HVCs in the MWG (Sancisi et al. 2008). This value, which reproduces well the infall prediction for the solar region, is, however, lower than expected when the total infall for the closest-to-MWG simulated galaxy (red or green line) is considered. In that case, the value of Lehner & Howk (2011) is, however, well reproduced. The value at $z = 0.375$ is an estimate obtained from the recent work by Fernández et al. (2016) who detect H I at the highest redshift, to date. They give the masses for the diffuse (and molecular gas), and use the stellar mass from *Spitzer* IRAC data: $M(\mathrm{H\,I}) = 2 \times 10^{10}$ $M_\odot$, the molecular one is $M(\mathrm{H_2}) = 1.8$–9.9×10^{10} $M_\odot$, and the stellar mass $M_* = 8.7 \times 10^{10}$ $M_\odot$. Using these numbers, a total disc mass is estimated in the range $[13.4$–$21.5] \times 10^{10}\,M_\odot$. If the disc accreted this mass in ∼8 Gyr (the evolutionary time from $z \sim 7$ to today), the averaged value for the infall rate would be ∼17–27 $M_\odot$ yr^{-1}. Taking into account that this is an averaged value across the full redshift range, and that the infall rate probably was greater at higher redshift, we reduce the value by a factor of two, that is $\log(\mathrm{d}M/\mathrm{d}t) \sim 1.00$. We note that taking into account the total mass of the disc, this galaxy would lie between our models 11 and 13, corresponding to $\log M_{\rm vir} = 12.25$ and 12.55 (represented by magenta and orange lines in the

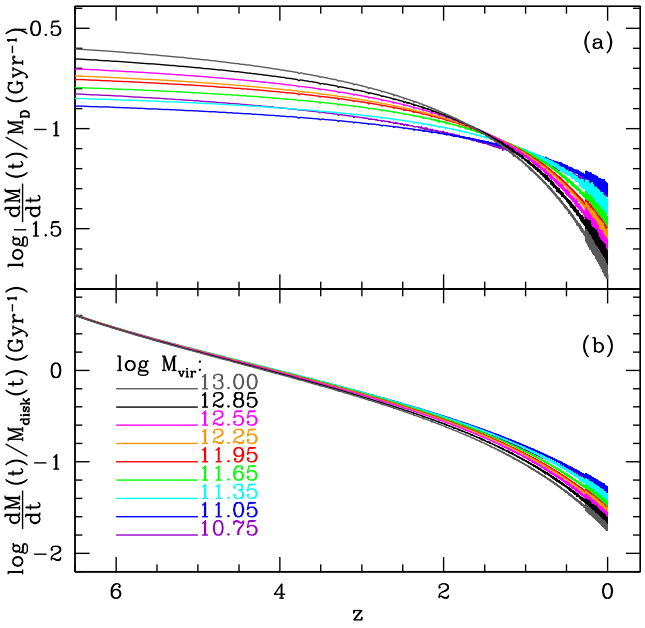

Figure 7. The infall rate normalized to (a) the final mass of the disc $\frac{dM}{dt}/M_D$, and (b) to the disc mass at each time $M_D(t)$, both in logarithmic scale, as a function of the redshift z for the same galaxies as shown in Fig. 6.

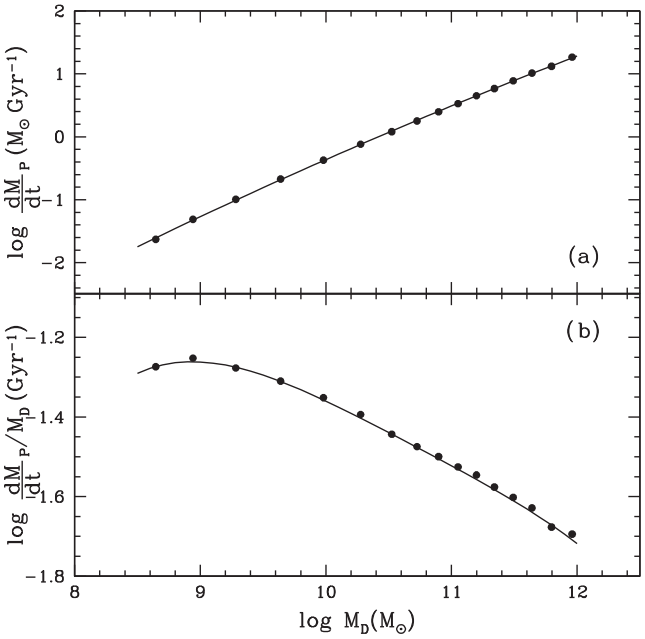

Figure 8. (a) The infall rate at the present time ($z = 0$), $(\frac{dM}{dt})_P$ and (b) as normalized to the final mass of the disc at the present time $(\frac{dM}{dt})_P/M_D$ as a function of disc mass M_D.

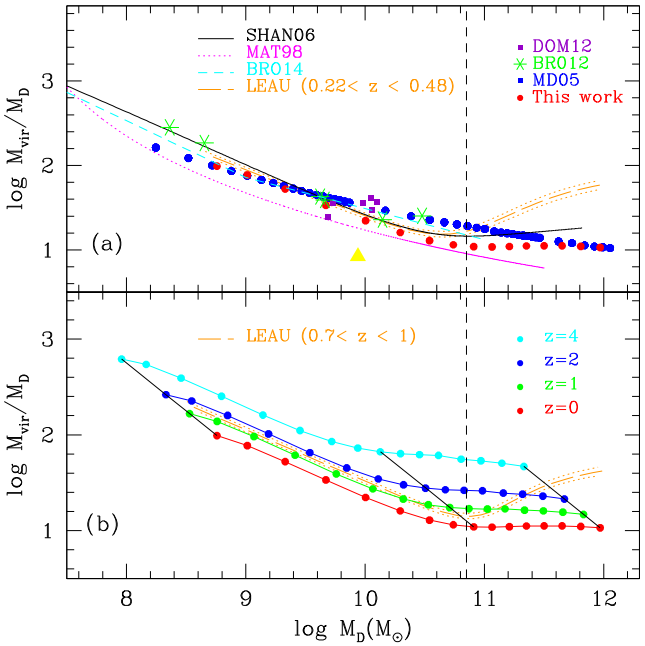

Figure 9. (a) The ratio $\frac{M_{vir}}{M_D}$ at $z = 0$ as a function of the mass in the disc M_D. Our models, calculated to follow the SHAN06 prescription (black line), are the red dots, while the blue dots are the MD05 results. The magenta, cyan, and black lines are the prescriptions obtained by Mateo (1998), labelled as MAT98, and from BRO14 and SHAN06 from observations of the Local Group of galaxies for the first two, and from halo distribution data, for the latter. The orange line shows results from LEAU for COSMOS data for the lowest redshift range. Cosmological simulations are drawn with purple squares and green stars from DOM12 and BRO12, respectively; (b) our results for the ratio $\frac{M_{vir}}{M_D}$ at $z = 0$, 1, 2, and 4, represented with different colours, as labelled, as a function of the mass in the disc M_D at each time, compared with results from LEAU for $z \sim 0.7 - 1.0$ (orange dashed line). Black lines join the evolutionary tracks for individual galaxies with $\log M_{vir} = 10.75$, 11.95, and 13.00.

accompanying figure). We see that these recent observational data compares very well with our model predictions.

The infall rate behaviour is very similar for all galaxy masses, with differences mainly in the absolute value. As such, we have normalized the infall rate to the mass of the disc, and show the results in Fig. 7. In (a) we normalize to the final disc mass M_D while in panel (b) we normalize to the disc mass at each time $M_D(t)$. We see that in panel (a) all infall rates coincide to the same value $\frac{dM}{dt}/M_D \sim 0.1\,\mathrm{Gyr}^{-1}$, at $z = 1.3$, while in panel (b) it is clear that the last normalized infall rate is practically the same for $z > 2.5$. This means that at high redshift, discs grow in the same proportion for all virial masses and it is only recently that differences appear.

The infall rate at the present time shows a correlation with the virial mass of the dark halo or with the mass in the disc M_D, as we show in Fig. 8. In panel (a), we see that the infall rate depends on the mass, increasing with M_D. However, in panel (b), where the normalized infall rate is represented, the contrary occurs: low mass galaxies are now suffering a higher infall rate in proportion to the total mass of their discs, while the massive discs have now a very low rate (almost an order of magnitude lower). This is again in agreement with the scenario where low-mass galaxies form their discs well after the most massive ones (the latter of which create their discs rapidly).

3.3 The growth of spiral discs

As a consequence of this gas infall scenario, the disc is formed in an inside-out fashion. The proportion of the final mass in the disc compared with the total dynamical mass of the galaxy is dependent on this total mass, in a consistent way to our inputs for calculating M_D (included as parameter in the RCs).

Panel (a) of Fig. 9 shows the fraction of the virial to the disc mass, $\frac{M_{vir}}{M_D}$, resulting from the applied collapse time-scale prescriptions of our new grid (red points), compared with our previous results from Mollá & Díaz (2005; blue points). We also show the relationship from Mateo (1998), and from Brook et al. (2014,

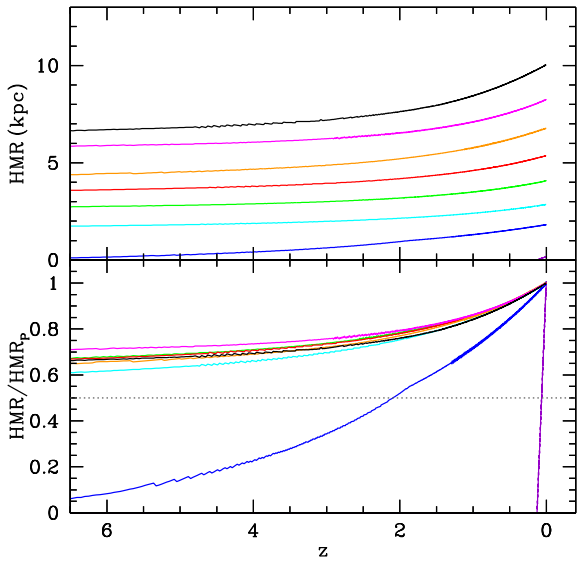

Figure 10. (a) The evolution of the radius enclosing the half baryonic mass of disc, *HMR*, with redshift z. (b) The redshift evolution of the same half-mass radii, normalized to their final value. Colour lines have the same coding as in Fig. 1.

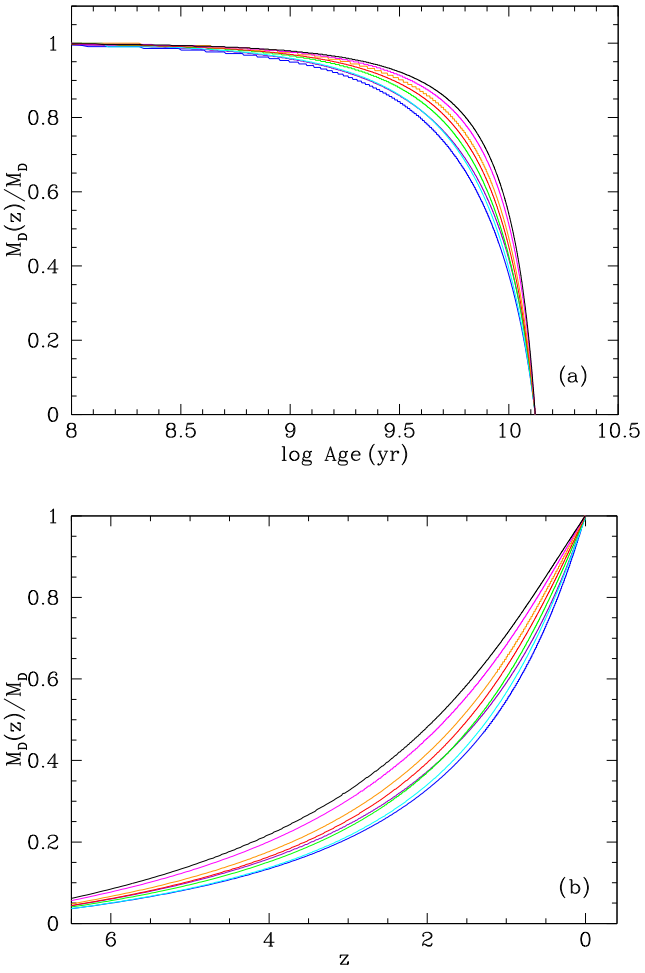

Figure 11. The evolution of the masses of discs normalized to their final values as a function: (a) of the disc age in logarithmic scale; (b) of the redshift.

hereinafter BRO14), both obtained for galaxies of the Local Group. Our older results from MD95 had a similar slope to the one from Mateo (1998), but the absolute value given by the latter is somewhat smaller, which is due to the M_*/L-ratio employed to transform the observations (luminosities) to stellar masses. The cosmological simulations begin to be able to predict discs of the appropriate size. We have drawn in the same Fig. 9, the results obtained by Doménech-Moral et al. (2012, hereinafter DOM12) and by Brook et al. (2012b, hereinafter BRO12). We also plot the results obtained by Leauthaud et al. (2010, hereinafter LEAU), who studied the SHMR using COSMOS data, for the lowest redshift they give (as labelled in the figure). Our new models are calculated to predict the line from SHAN06 and are close to the one from LEAU, and, in excellent agreement with DOM12, BRO12, and BRO14. In the cases of LEAU and SHAN06, lines show an increase for high disc masses which, obviously, is not apparent in our old models, since we had assumed a continuous dependence of the collapse time-scale with the dynamical mass. This increase is, however, rather modest for the SHAN06 line and the models follow this trend. In panel (b) of the same figure we show our results for redshifts $z = 0$, 1, 2, and 4, with different colours, as labelled. The relation looks similar for $z \leq 2$, however, when we see the track for a particular galaxy, shown by black lines for three values of $\log M_{\rm vir} = 10.75$, 11.95, and 13.00, the evolution is clear, with decreasing ratios $M_{\rm vir}/M_{\rm D}$ for increasing $M_{\rm D}$. Results for $z = 1$ are close to the LEAU data for the range $0.7 < z < 1.0$.

Fig. 10 shows the evolution of the half (baryonic) mass radius of the disc, *HMR*, with redshift, for the same galaxies of Fig. 1. This figure also supports the notion that the growth of massive discs is more rapid than the growth of the low mass ones (which are still forming their discs). In panel (a) we see directly the redshift evolution of these HMRs. Clearly, the lowest mass galaxies evolve very late compared with the others. This difference of behaviour is even clearer in panel (b), where the HMRs are normalized to their final value reached at the end of the evolution (or the present time), $HMR_{\rm P}$. In that case, most of galaxies show a similar evolution, except the lowest mass galaxies, which have very separated evolutionary tracks.

We also check how the discs grow by comparing the fraction of the final disc mass which is in place at each redshift in Fig. 11. Obviously, all tracks end at a value of unity at $z = 0$ (100 per cent of $M_{\rm D}$ in the present time), but the evolution differs for each galaxy depending on the virial mass. This kind of plot is similar to that obtained by Pérez et al. (2013), for the Calar Alto Legacy Integral Field Area survey (Sánchez et al. 2012) galaxies as shown in panel (a), where we represent the proportion of the total mass placed in the disc as a function of the disc age, equal to $13.8 - t$, t being the evolutionary time. In panel (b) the same is shown as a function of the redshift z.

On the other hand we may also compare the final $HMR_{\rm P}$ or radius at the present time, for different galaxies. Panel (a) of Fig. 12 plots $HMR_{\rm P}$ as a function of the disc mass, $M_{\rm D}$, also at the present time. Clearly, there is a relationship between the baryonic mass in discs and their sizes, measured by the $HMR_{\rm P}$, as expected. Actually, by assuming that discs are exponential and using these quantities, we also might calculate the surface density at the centre of the galaxy as $\Sigma_0 = \frac{M_{\rm D}}{4\pi R^2}$. We plot this surface density, Σ_0, as a function of the disc mass in panel (b) of the same Fig. 12, where points show a smooth behaviour.

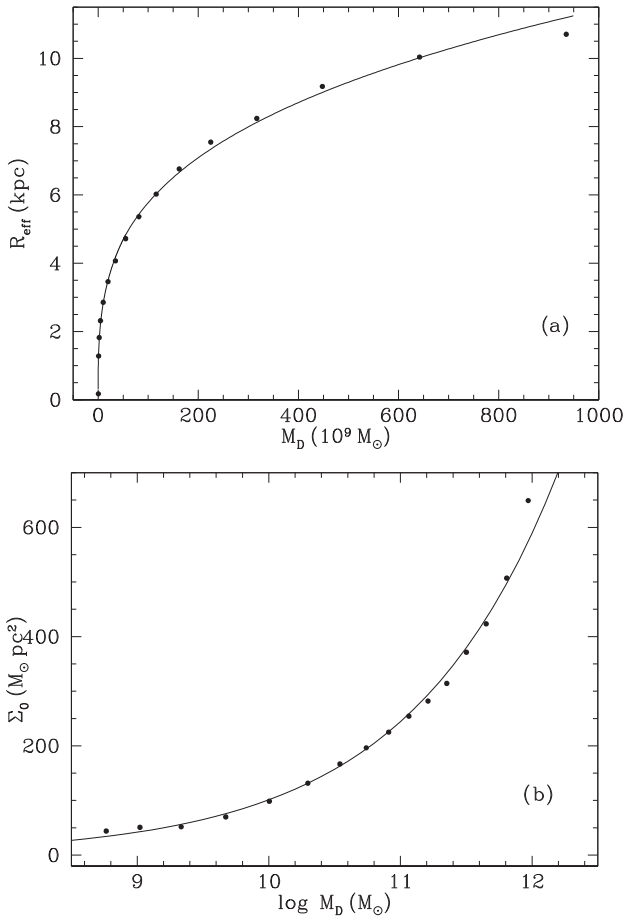

Figure 12. (a) The present half-mass radius HMR_P and (b) the present central surface density Σ_0, as a function of the final mass of disc M_D, on a logarithmic scale.

4 DISCUSSION

By imposing the final disc mass distributions resemble those from SAL07, we have computed the infall rates in the discs of spiral galaxies. From our models, we have reached important results regarding the mass assembly in disc galaxies compared with previous results in the literature. The new prescriptions adopted in this work resulted in a MWG analogue where radial regions with $R > 10$ kpc have collapse time-scales larger than the Hubble time (see Fig. 2). Other radial functions for τ in the literature have also suggested these time-scales are reached at comparable ∼10–15 kpc galactocentric radii; as such, a larger portion of the outer Disc in our new MWG analogue is still currently assembling, compared to conclusions which would be drawn with most of the previously available time-scales in the literature. In Fig. 3, a clear dependence of the gas infall rate on redshift, and also on radius, appears except for the outer disc regions where the infall rate is almost constant in spite of redshift variations. At the inner disc regions and the bulge, however, the cold gas accretion is higher at high redshifts than now. This cold gas accretion in the inner regions of high-redshift galaxies is supported by observations: Cresci et al. (2010) find that a massive infall of gas in the central regions of high-redshift galaxies ($z \sim 2-3$) is needed to explain the gas metallicity distribution within these galaxies. In the local Universe there is also evidence that there still exists cold gas accretion in disc galaxies (e.g. Sánchez Almeida et al. 2014b, and references therein).

With our collapse time-scales varying with R, the resulting discs are also created in agreement with the inside-out formation scenario. Following Fig. 3, the inner regions of a galaxy are formed faster than the outer ones, while these latter present infall rates which are less variable with redshift. In agreement with this, the outer regions of the MWG analogue model are still accreting gas. This new result is in agreement with surveys of extended UV discs around both early- and late-type galaxies in the local Universe that suggest gas accretion in their outer parts (Lemonias et al. 2011; Moffett et al. 2012). In fact, these latter authors establish that gas-rich galaxies below a stellar mass of $M_* \sim 5 \times 10^9$ $M_\odot$ display UV-bright discs, supporting an active disc growth. This limit is basically the value in which $\tau_c > T_{UNIVERSE}$ in our models, as seen in Table 1, between models 4 and 5. This limit in the collapse time-scale also appears when considering the different radial regions within discs, thus suggesting that these discs may continue growing at the present time even in the most massive galaxies.

Another important result that we have obtained is the dependence on redshift of the infall rate normalized to the disc mass in each time-step for different M_{vir}, shown in Fig. 8. The gas accretion profile is similar for all simulated galaxies at $z > 2$, and only for lower redshifts does the infall rate depend on M_{vir}. This has important implications for how discs grow their masses at high redshifts. Since galaxies form and evolve by accreting gas from their surroundings, our models suggest that the accretion of gas is similar for spiral galaxies, regardless of their masses. Kereš et al. (2009) showed that cold mode accretion via filaments is responsible for the supply of gas in galaxies. Kereš & Hernquist (2009) showed that the gas is accreted via filaments from the intergalactic medium and these filaments can condense into clouds and provide gas for star formation. These clouds may be analogues of HVCs surrounding the MWG which are thought to provide the fuel for star formation in the Galaxy. Therefore, the similarity between the accretion rates found here for spiral galaxies with different M_{vir} suggests an analogous disc growth for these galaxies and, consequently, similar disc properties. We will analyse these properties, as the possible formation of stars in the outer regions of discs or the variations of radial gradients of abundances, in a future work (Mollá et al., in preparation). Therein, we will take into account the star formation processes and the consequent metal enrichment, not included yet here, when the chemical evolution computed is computed self-consistently.

5 CONCLUSIONS

In this work, we have presented the infall rates used as input to a grid of chemical models for spiral galaxies. We also performed a systematic comparison with data and competing models in the literature, including cosmological simulations. Our main conclusions can be summarized as follows.

(i) The more massive the galaxy, the higher the absolute value of the infall rate at all redshifts.

(ii) The infall rates necessary to reproduce the relationship between $M_{vir}-M_D$ are smoother than the ones assumed in classical CEMs, including our earlier generation of models (MD05). They are also lower and smoother than the accretion rates produced in cosmological simulations which create spheroids and are in better agreement with those resulting in realistic late-type discs (employing contemporary prescriptions for star formation and feedback).

(iii) The evolution of the infall rate with redshift is quite constant for discs, decreasing smoothly for $z < 2$ and showing very similar behaviour for all radial regions, with differences only in the absolute

value. This smooth evolution is different than the steep decline with redshift shown for bulges.

(iv) The normalized infall rate is essentially the same for all discs until $z = 2$, and shows only small differences for $z < 2$.

(v) The final relationship among disc and halo masses, denoted as SHMR, obtained by these new prescriptions, agrees well with observations and cosmological simulations.

(vi) From redshift $z = 2.5$ to today, discs grow in size by a factor of 2 (except for the lowest mass galaxies), while the disc masses increase by a factor of 5 to 10.

(vii) These infall rates (decreasing with time and with radius within each theoretical galaxy) are in agreement with the classical inside-out scenario, and also with the cosmological simulations infall rates from Courty et al. (2010).

(viii) The growth of discs continue to the present time, with gas accretion across the discs of low mass systems, and in the outer regions of more massive spirals.

ACKNOWLEDGEMENTS

We gratefully acknowledge the advice of the referee which improved the manuscript dramatically. This work has been supported by DGICYT grant AYA2010-21887-C04-02 and AYA2013-47742-C4-4-P. MM thanks the kind hospitality and wonderful welcome of the Jeremiah Horrocks Institute at the University of Central Lancashire, the E.A. Milne Centre for Astrophysics at the University of Hull, and the Instituto de Astronomia, Geofísica e Ciências Atmosféricas in São Paulo (Brazil), where this work was partially done. This work has been supported financially by grant 2012/22236-3 from the São Paulo Research Foundation (FAPESP). This work has made use of the computing facilities of the Laboratory of Astroinformatics (IAG/USP, NAT/Unicsul), whose purchase was made possible by the Brazilian agency FAPESP (grant 2009/54006-4) and the INCT-A. We acknowledge PRACE, through its Distributed Extreme Computing Initiative, for resource allocations on Sisu (CSC, Finland), Archer (EPCC, UK), and Beskow (KTH, Sweden). We acknowledge the support of STFC DiRAC High Performance Computing Facilities; DiRAC is part of the UK National E-infrastructure.

REFERENCES

Balcells M., Graham A. W., Peletier R. F., 2007, ApJ, 665, 1104
Barbieri C. V., Fraternali F., Oosterloo T., Bertin G., Boomsma R., Sancisi R., 2005, A&A, 439, 947
Behroozi P. S., Conroy C., Wechsler R. H., 2010, ApJ, 717, 379
Behroozi P. S., Wechsler R. H., Conroy C., 2013, ApJ, 770, 57
Blitz L., Spergel D. N., Teuben P. J., Hartmann D., Burton W. B., 1999, ApJ, 514, 818
Boissier S., Prantzos N., 1999, MNRAS, 307, 857 (B&P99)
Boissier S., Prantzos N., 2000, MNRAS, 312, 398
Boomsma R., Oosterloo T. A., Fraternali F., van der Hulst J. M., Sancisi R., 2008, A&A, 490, 555
Brook C. B. et al., 2012a, MNRAS, 426, 690
Brook C. B., Stinson G., Gibson B. K., Wadsley J., Quinn T., 2012b, MNRAS, 424, 1275 (BRO12)
Brook C. B., Di Cintio A., Knebe A., Gottlöber S., Hoffman Y., Yepes G., Garrison-Kimmel S., 2014, ApJ, 784, L14 (BRO14)
Burkert A., 1995, ApJ, 447, L25
Carigi L., Peimbert M., 2008, Rev. Mex. Astron. Astrofis., 44, 341 (CAR08)
Chan M. H., 2013, Ap&SS, 345, 195
Chang R. X., Hou J. L., Shu C. G., Fu C. Q., 1999, A&A, 350, 38 (CHA99)
Chiappini C., Matteucci F., Gratton R., 1997, ApJ, 477, 765
Chiappini C., Matteucci F., Romano D., 2001, ApJ, 554, 1044 (CHIA01)
Chiappini C., Matteucci F., Meynet G., 2003, A&A, 410, 257
Connors T. W., Kawata D., Bailin J., Tumlinson J., Gibson B. K., 2006, ApJ, 646, L53
Courty S., Gibson B. K., Teyssier R., 2010, in Debattista V. P., Popescu C. C., eds, AIP Conf. Ser. Vol. 1240, Hunting for the Dark: The Hidden Side of Galaxy Formation. Am. Inst. Phys., New York, p. 131
Cresci G., Mannucci F., Maiolino R., Marconi A., Gnerucci A., Magrini L., 2010, Nature, 467, 811
Dekel A., Sari R., Ceverino D., 2009, ApJ, 703, 785 (DEK09)
Doménech-Moral M., Martínez-Serrano F. J., Domínguez-Tenreiro R., Serna A., 2012, MNRAS, 421, 2510 (DOM12)
Donato F. et al., 2009, MNRAS, 397, 1169
Edmunds M. G., 1990, MNRAS, 246, 678
Faucher-Giguère C.-A., Kereš D., Ma C.-P., 2011, MNRAS, 417, 2982 (FG11)
Fenner Y., Gibson B. K., 2006, Publ. Astron. Soc. Aust., 20, 189
Fernández X. et al., 2016, ApJ, 824, L1
Ferrini F., Matteucci F., Pardi C., Penco U., 1992, ApJ, 387, 138
Ferrini F., Molla M., Pardi M. C., Diaz A. I., 1994, ApJ, 427, 745
Fraternali F., Cappi M., Sancisi R., Oosterloo T., 2002, ApJ, 578, 109
Freeman K. C., 1970, ApJ, 160, 811
Gallagher J. S., III, Hunter D. A., Tutukov A. V., 1984, ApJ, 284, 544
Ganda K., Peletier R. F., Balcells M., Falcón-Barroso J., 2009, MNRAS, 395, 1669
Gentile G. et al., 2013, A&A, 554, A125
Gibson B. K., Giroux M. L., Penton S. V., Stocke J. T., Shull J. M., Tumlinson J., 2001, AJ, 122, 3280
Guo Q., White S., Li C., Boylan-Kolchin M., 2010, MNRAS, 404, 1111
Güsten R., Mezger P. G., 1983, Vistas Astron., 26, 159
Heald G. et al., 2011, A&A, 526, A118
Heavens A., Panter B., Jimenez R., Dunlop J., 2004, Nature, 428, 625
Kereš D., Hernquist L., 2009, ApJ, 700, L1
Kereš D., Katz N., Fardal M., Davé R., Weinberg D. H., 2009, MNRAS, 395, 160
Kormendy J., Freeman K. C., 2016, ApJ, 817, 84
Lacey C. G., Fall S. M., 1983, MNRAS, 204, 791
Lacey C. G., Fall S. M., 1985, ApJ, 290, 154
Larson R. B., 1972, NPhS, 236, 7
Leauthaud A. et al., 2010, ApJ, 709, 97 (LEAU)
Lehner N., Howk J. C., 2011, Science, 334, 955
Lemonias J. J. et al., 2011, ApJ, 733, 74
López-Sánchez Á. R., 2010, A&A, 521, A63
López-Sánchez Á. R., Koribalski B. S., van Eymeren J., Esteban C., Kirby E., Jerjen H., Lonsdale N., 2012, MNRAS, 419, 1051
Lynden-Bell D., 1975, Vistas Astron., 19, 299
MacDonald A., 2006, Found. Phys. Lett., 19, 631
Marcon-Uchida M. M., Matteucci F., Costa R. D. D., 2010, A&A, 520, A35 (MAR10)
Mateo M. L., 1998, ARA&A, 36, 435
Matteucci F., Francois P., 1989, MNRAS, 239, 885
Micali A., Matteucci F., Romano D., 2013, MNRAS, 436, 1648
Moffett A. J., Kannappan S. J., Baker A. J., Laine S., 2012, ApJ, 745, 34
Mollá M., Díaz A. I., 2005, MNRAS, 358, 521
Mollá M., Ferrini F., Díaz A. I., 1996, ApJ, 466, 668
Moster B. P., Somerville R. S., Maulbetsch C., van den Bosch F. C., Macciò A. V., Naab T., Oser L., 2010, ApJ, 710, 903
Navarro J. F., Frenk C. S., White S. D. M., 1996, ApJ, 462, 563 (NFW)
Nelson D. et al., 2015a, Astron. Comput., 13, 12
Nelson D., Genel S., Vogelsberger M., Springel V., Sijacki D., Torrey P., Hernquist L., 2015b, MNRAS, 448, 59 (NEL15)
Nelson D., Genel S., Pillepich A., Vogelsberger M., Springel V., Hernquist L., 2016, MNRAS, 460, 2881
Nesti F., Salucci P., 2013, J. Cosmol. Astropart. Phys., 7, 16
Ogiya G., Mori M., 2014, ApJ, 793, 46
Ogiya G., Mori M., Ishiyama T., Burkert A., 2014, MNRAS, 440, L71
Oosterloo T., 2004, in van Woerden H., ed., Astrophysics and Space Science Library, Vol. 312, High Velocity Clouds. Kluwer, Dordrecht, p. 125
Pérez E. et al., 2013, ApJ, 764, L1

Pérez-González P. G. et al., 2008, ApJ, 675, 234
Persic M., Salucci P., Stel F., 1996, MNRAS, 281, 27
Portinari L., Chiosi C., Bressan A., 1998, A&A, 334, 505
Renda A., Kawata D., Fenner Y., Gibson B. K., 2005, MNRAS, 356, 1071 (REN05)
Richter P., 2006, Rev. Mod. Astron., 19, 31
Richter P., 2012, ApJ, 750, 165
Rodríguez-Puebla A., Drory N., Avila-Reese V., 2012, ApJ, 756, 2
Rodríguez-Puebla A., Avila-Reese V., Yang X., Foucaud S., Drory N., Jing Y. P., 2015, ApJ, 799, 130
Salucci P., Lapi A., Tonini C., Gentile G., Yegorova I., Klein U., 2007, MNRAS, 378, 41 (SAL07)
Sánchez Almeida J., Elmegreen B. G., Muñoz-Tuñón C., Elmegreen D. M., 2014a, A&AR, 22, 71
Sánchez Almeida J., Morales-Luis A. B., Muñoz-Tuñón C., Elmegreen D. M., Elmegreen B. G., Mééndez-Abreu J., 2014b, ApJ, 783, 45
Sánchez S. F. et al., 2012, A&A, 538, A8
Sancisi R., Fraternali F., Oosterloo T., van der Hulst T., 2008, A&AR, 15, 189
Schaye J. et al., 2015, MNRAS, 446, 521
Schmidt M., 1963, ApJ, 137, 758
Shankar F., Lapi A., Salucci P., De Zotti G., Danese L., 2006, ApJ, 643, 14 (SHAN06)
van den Bergh S., 1962, AJ, 67, 486
Vogelsberger M., Genel S., Sijacki D., Torrey P., Springel V., Hernquist L., 2013, MNRAS, 436, 3031
Wakker B. P., van Woerden H., Gibson B. K., 1999, ASP Conf. Ser. Vol. 166, Astron. Soc. Pac., San Francisco, p. 311
Worthey G., Dorman B., Jones L. A., 1996, AJ, 112, 948
Yang X., Mo H. J., van den Bosch F. C., Zhang Y., Han J., 2012, ApJ, 752, 41
Yegorova I. A., Babic A., Salucci P., Spekkens K., Pizzella A., 2012, A&AT, 27, 335

This paper has been typeset from a TEX/LATEX file prepared by the author.